ARTICLE

Is Cs_2TiBr_6 a promising Pb-free perovskite for solar energy applications?

Received 00th January 20xx,
Accepted 00th January 20xx

DOI: 10.1039/x0xx00000x

Julie Euvrard,[a] Xiaoming Wang,[b] Tianyang Li,[a] Yanfa Yan [b] and David B. Mitzi *[a,c]

In a quest for Pb-free perovskites suitable for solar energy applications, Cs_2TiBr_6 has recently been reported as a promising compound showing appropriate optical and electrical properties as well as high stability under environmental stresses. In this study, we pursue investigation on this compound, demonstrating phase pure Cs_2TiBr_6 powder formation using solution synthesis and providing complementary experimental characterization and theoretical calculations. An experimental absorption onset of around 2.0 eV is extracted and a weak broad photoluminescence is measured. Density functional theory calculations predict an indirect bandgap, parity-forbidden for both the direct and indirect transitions, which explains the weak and Stokes shifted luminescence. Additionally, we highlight the strong instability of Cs_2TiBr_6 powder in ambient atmosphere. Therefore, our experimental results supported by theoretical calculations differ from previous results and raise doubts on the suitability of Cs_2TiBr_6 in its pristine form for solar energy applications.

Introduction

Among the emergent materials studied to develop the future generation of solar cells, Pb-based perovskites have shown the most promising performance metrics, resulting in a rapid rise in solar cell power conversion efficiency, now exceeding 25%.[1,2] Although very exciting, the rapid development of perovskite-based devices is facing two major challenges for commercialization: lead toxicity and poor stability.[3,4] Pb-based perovskites with the 3D structure ABX_3 (e.g., A: $CH_3NH_3^+$ or Cs^+, B: Pb^{2+}, X: I^- or Br^-) remain the most efficient compounds for use in solar absorbers and extensive efforts are underway to find alternative Pb-free compounds with promising properties.[5,6] Unfortunately, solar cells fabricated with Pb-free perovskites exhibit limited efficiency and the development of appropriate compounds (good optical and transport properties, good stability) is not a straightforward task. Sn and Ge-based 3D perovskites are unstable due to their propensity to self-dope upon air exposure through the facile oxidation of Sn^{2+} and Ge^{2+} into Sn^{4+} and Ge^{4+}.[5] Inorganic Bi and Sb-based perovskites with lower dimensionality are also explored to substitute Pb, showing good stability but poor power conversion efficiencies (PCE) when integrated in a solar cell device.[6] As 3D perovskite structures appear to hold more promise in terms of device performance than 2D systems, double perovskites such as $Cs_2BiAgBr_6$ have also been developed.[7]

In this quest for new Pb-free perovskites, Cs_2TiBr_6 has recently been reported as a promising compound, leading to solar cell efficiencies of as high as 3.3%.[8,9] With a reported experimental bandgap of 1.8 eV, this compound could be appropriate for tandem devices. Additionally, intense photoluminescence suggests low nonradiative recombination rate and diffusion lengths above 100 nm have been extracted. A very good stability has also been reported under thermal stress and exposure to light and humid environment. The combination of so many favorable properties for solar energy applications makes Cs_2TiBr_6 a very strong candidate for Pb-free perovskite solar cells. Very recently, a new study reported experimental data on Cs_2TiBr_6 film that differ from the initial results, although the ability of this compound to be used in solar cells and other applications is not called into question.[10] In a hope to further understand and optimize this compound, we have synthesized and characterized phase-pure Cs_2TiBr_6 powder using a solution synthesis approach as an alternative to solid state synthesis. Additionally, theoretical calculations using density functional theory (DFT) have been performed to support and understand our experimental observations. Our experimental and theoretical findings differ from previously reported results. We show the formation of phase-pure Cs_2TiBr_6 powder, with XRD pattern fully consistent with DFT calculations and exhibiting a lattice constant of 10.69 Å, approximately 0.2 Å smaller than the lattice constant reported in an earlier study[9] but consistent with a recent study from Kong et al.[10] We obtain an experimental absorption onset of around 2.0 eV and a weak photoluminescence response. DFT calculations are consistent with our experimental absorption spectrum and provide insight into the origin of the limited photoluminescence through the indirect and parity-forbidden transitions. Finally, we highlight

[a] Department of Mechanical Engineering and Materials Science, Duke University, Durham, North Carolina 27708, United States.
[b] Department of Physics and Astronomy and Wright Center for Photovoltaics Innovation and Commercialization, The University of Toledo, Toledo, Ohio 43606, United State.
[c] Department of Chemistry, Duke University, Durham, North Carolina 27708, United States.

† Footnotes relating to the title and/or authors should appear here.
Electronic Supplementary Information (ESI) available: [details of any supplementary information available should be included here]. See DOI: 10.1039/x0xx00000x

the high instability of Cs_2TiBr_6 powder in ambient atmosphere, raising doubts as to the suitability of this compound for solar energy applications.

Experimental

Synthesis

Cs_2TiBr_6 is synthesized by reaction of CsBr (0.5 mmol) and $TiBr_4$ (0.3 mmol, 20 mol% excess) in 1 mL HBr (48 wt%) at 100°C for 12 hours in a closed vial in air. The solid liquid mixture is then centrifuged and the liquid subsequently discarded. The resulting red powder is vacuum dried to remove remaining solvent and excess $TiBr_4$, without exposing the Cs_2TiBr_6 powder to ambient atmosphere. The dry powder is annealed in the glovebox at 100°C for 30 min to improve the crystallinity. Additionally, the annealing step is expected to separate the final powder from potential $TiBr_4$ residues, taking advantage of the reactant's high volatility and low melting point (39°C).

Characterization

X-ray diffraction measurements of Cs_2TiBr_6 powder were obtained with a PANalytical Empyrean powder X-ray diffractometer using a Cu Kα X-ray source operating at 45 kV/40 mA. To prevent the impact of ambient atmosphere, initial spectra were recorded on powder covered with a thin (.0003'') Kapton film, sealed to the glass substrate with double-sided Kapton tape. To follow the impact of ambient atmosphere, XRD spectra were subsequently recorded after removal of the Kapton film protection (each scan takes 10 min). The fitting of the XRD patterns was performed using the HighScore Plus software package. Diffuse reflectance measurements were carried out on an Enlitech QE-R Quantum Efficiency/Reflectivity system with integrating sphere. The absorption spectrum is calculated using the Kubelka-Munk theory. Photoluminescence (PL) measurements were performed with an Horiba Jobin Yvon LabRam ARAMIS system using a 442 nm HeCd laser as excitation. Diffuse reflectance and PL measurements were carried out at room temperature and in ambient atmosphere (between 45 and 50% RH). To limit the impact of ambient atmosphere, the powder was maintained in a sealed vial until the corresponding measurement. As a result, Kubelka-Munk (KM) and PL spectra were recorded on a powder exposed to ambient atmosphere for about 1-2 min. Thermogravimetric analysis (TGA) measurement was performed on a TA Q50 instrument using a ramping rate of 5 ˚C/min from 25 ˚C to 500 ˚C, under nitrogen gas flow, and with a 16 mg sample size.

DFT calculations

Density functional theory calculations were performed using the VASP code[11,12] with projector augmented-wave (PAW)[13] potentials. A kinetic energy cutoff of 500 eV, Γ-centered $4 \times 4 \times 4$ k-mesh, and PBEsol functional were employed. The crystal structure was relaxed with force tolerance of 0.01 eV/Å. The band symmetries are analyzed with the Quantum ESPRESSO package[14] with GBRV pseudopotentionals.[15]

Results

Solid state synthesis of Cs_2TiBr_6 powder and thin film formation using a vapor-solid reaction have been previously reported in the literature.[8,9] In this work we use a solution synthesis approach as an alternative route in the formation of phase-pure Cs_2TiBr_6 powder. The CsBr and $TiBr_4$ precursors are mixed in HBr solution with a 20 mol% excess of $TiBr_4$ to prevent incomplete reaction due to the high volatility of this reactant. To avoid the impact of ambient atmosphere and remove the excess $TiBr_4$, the final dark red powder is vacuum dried and transferred to the glovebox in a sealed tube. Subsequent thermal treatments are performed to increase the crystallinity of the powder and ensure total removal of excess $TiBr_4$. The choice of the temperature needs to be finely tuned to avoid the decomposition of the product. Fig. 1a compares the XRD spectra of Cs_2TiBr_6 powder obtained directly after drying and with subsequent annealing treatments at 100°C and 250°C for 30 min. When no thermal treatment is used on the Cs_2TiBr_6 powder, peak splitting can be observed suggesting the presence of an additional phase with a different lattice constant. Using Bragg's law on the higher angle peaks, a lattice constant of 10.57±0.01 Å is obtained, consistent with the value reported by Kozhina and Korol'kov,[16] which they obtained by measuring in argon atmosphere. It is worth noting that this phase is highly unstable in ambient atmosphere as the higher angle peaks disappear directly after removal of the protective Kapton film (Figure S1). After a thermal treatment at 100°C, only the lower angle peaks are observed and the crystallinity is improved (according to the peak intensity). Increasing further the annealing temperature to 250°C results in the formation of a small additional peak at 29.5° corresponding to the CsBr phase without further improvement of the crystallinity. Therefore, a temperature of 100°C is chosen for the thermal treatment of the Cs_2TiBr_6 powder. Fig 1b displays the simulated and experimental XRD patterns obtained under a thin protective Kapton film and the Pawley fitting using a cubic Fm-3m crystal structure is given in Supplementary Information (Figure S2). All peaks observed can be accounted for as Cs_2TiBr_6 and a goodness-of-fit of 0.99 is obtained with a small difference between experimental and calculated patterns. A unit cell parameter of a=10.6907±0.0005 Å results from the Pawley fitting, approximately 0.2 Å lower than the value of 10.92 Å previously reported by Ju et al.[9], approximately 0.1 Å higher than the value of 10.57 Å reported by Kozhina and Korol'kov[16] and consistent with the lattice constant recently extracted by Kong et al.[10] The simulated XRD pattern shown in Fig 1b is obtained from the Cs_2TiBr_6 cubic unit cell after full relaxation using DFT calculations based on PBEsol[17] functionals (computational results will be discussed in more detail below). The DFT-relaxed lattice constant a=10.62 Å, close to the experimental value, and the peak relative intensities are consistent between the two patterns.

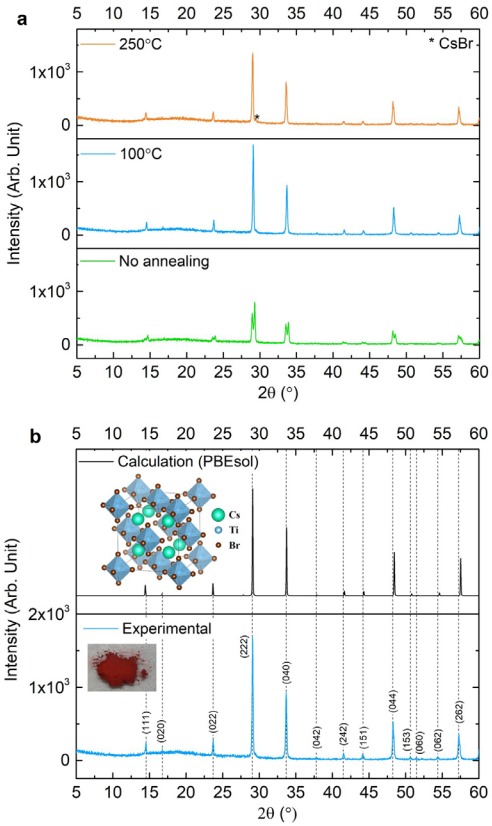

Fig. 1. (a) XRD spectra of the Cs_2TiBr_6 powder obtained by solution synthesis without subsequent thermal treatment (green) and with a 30 min annealing at 100°C (blue) and 250°C (orange). (b) Comparison of measured XRD pattern of Cs_2TiBr_6 powder annealed at 100°C with the simulated XRD pattern based on the DFT(PBEsol)-relaxed structure. The crystal structure and a picture of the Cs_2TiBr_6 powder are given as insets. The picture is taken within 1 min of exposure to ambient atmosphere, with no visible degradation observed.

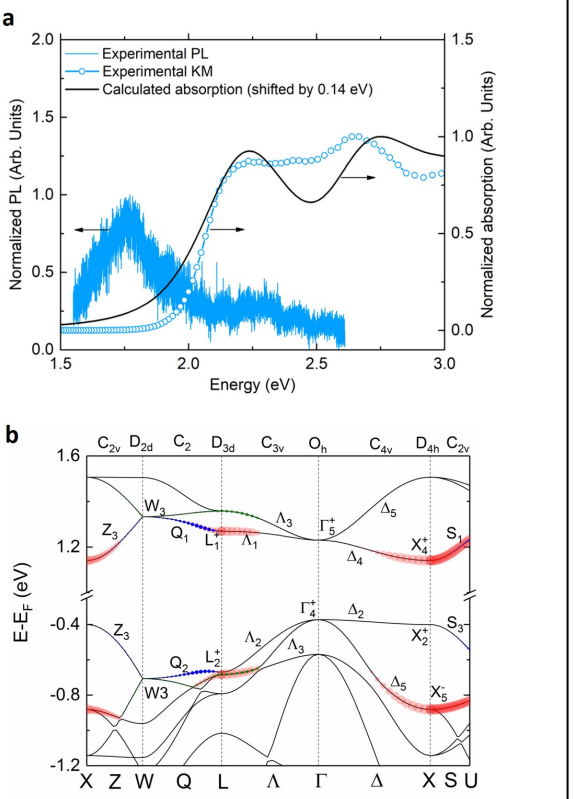

Fig. 2. (a) PL and absorption spectra obtained on Cs_2TiBr_6 powder. The absorption spectrum obtained experimentally is compared to the DFT-derived absorption spectrum shifted by 0.14 eV. (b) DFT band structure of Cs_2TiBr_6. Symmetry labels are shown for the corresponding points and lines. Group symbols for different k points are labelled on the top axis. The transition dipole moment squares, P2, between valence and conduction bands are plotted as fatbands.

The optical properties of the Cs_2TiBr_6 powder have been experimentally determined and compared to the theoretical predictions. The absorption spectrum of Cs_2TiBr_6 measured using diffuse reflectance is shown in Fig 2a. An onset around 2 eV is observed and a bandgap of between 1.9 eV (indirect) and 2 eV (direct) is extracted from the Tauc plots (see Supplementary Information Figure S3), consistent with the dark red color of the powder. Successive measurements performed on Cs_2TiBr_6 powder are displayed in Supplementary Information (Figure S4) and show a decrease and flattening of the absorption after a few minutes in ambient atmosphere while maintaining a similar bandgap. The photoluminescence of the Cs_2TiBr_6 powder (Fig. 2a) has been measured using an excitation wavelength of 442 nm and a silicon substrate to avoid any background signal (see Supplementary Information Figure S5 for the PL spectrum of the silicon substrate). Cs_2TiBr_6 powder exhibits a very weak and broad PL peak centered at 1.75 eV. A peak broadening and shift toward higher energy can be observed after ~3 min in ambient atmosphere (Figure S6) suggesting high instability of Cs_2TiBr_6 powder and will be further discussed below.

To understand the experimental findings, we evaluate the band structure (Fig. 2b) and optical absorption coefficient (Fig. 2a) through DFT calculations. For better comparison, the calculated absorption coefficient is shifted (0.14 eV) to align the first peak with the experimental data. The calculated DFT fundamental bandgap with indirect nature between Γ and X is 1.51 eV, which is 30 meV smaller than the direct bandgap at X. Underestimation of the bandgap is a well-known deficiency for DFT calculations due to the self-interaction error and our calculated band structure is consistent with previous calculations.[8,10] The band symmetries are labelled at high-symmetry points and lines in the band structure for better understanding the optical transition process. Both the indirect ($\Gamma_4^+ \rightarrow X_4^+$) and direct ($X_2^+ \rightarrow X_4^+$) transitions are found to be parity forbidden, consistent with the dipole forbidden transition proposed in the vacancy ordered double perovskite Cs_2SnI_6.[18] We also calculate the transition dipole moment squared, P^2, between the top two valance bands and bottom two conduction bands and plot P^2 in a fatband feature, i.e., the size of the color dots is proportional to P^2. As can be seen from Fig. 2b, for the top valence band to bottom conduction band transitions, the transitions from lines $\Lambda_2 \rightarrow \Lambda_1$ and $\Delta_2 \rightarrow \Delta_4$ are completely forbidden. In the vicinity of the X point, the transitions from lines $S_3 \rightarrow S_1$ and $Z_3 \rightarrow Z_3$ are only weakly allowed (blue dots). Therefore, very weak intensity for a

continuous photon energy range is expected starting from the fundamental absorption edge, as demonstrated by the imaginary part of the dielectric function ε_2 (Figure S7). The first intense absorption peak is expected to be for the $X_5^- \rightarrow X_4^+$ transition, which is ~0.5 eV higher than the fundamental bandgap, due to the large transition dipole moment (red dots) and density of states. The photoexcited electrons and holes would relax to the fundamental band edge through electron-phonon coupling very quickly. Hence, the PL should probe the fundamental band edge transitions (neglecting excitonic effects). The difference between the PL emission and the first absorption peak is found from experiment to be ~0.5 eV, which is consistent with our above theoretical analysis. Another possible reason for the Stokes shifted broadband emission is the formation of self-trapped excitons (STEs).[19] However, we didn't observe STEs in our calculations. Therefore, we can assign the PL emission at 1.75 eV to approximately correspond to fundamental band edge transitions. The broadness and weakness of the PL can be rationalized in the context of (multi-) phonon assisted indirect transitions and parity-forbidden transitions. Our experimental observations, consistent with theoretical calculations, contradict the previously reported[8,9] flat absorption spectrum between 600 nm (2.07 eV) and 450 nm (2.76 eV), direct bandgap of 1.8 eV and bright PL peak. However, the recent study from Kong et al.[10] shows a weak and broad PL for Cs_2TiBr_6, consistent with our observation. These results therefore call into question the suitability of Cs_2TiBr_6 for solar cell applications due to the unsuitable optical properties.

As a last step in the characterization of Cs_2TiBr_6 powder synthesized in solution, we evaluate its intrinsic and environmental stability. XRD patterns over time of Cs_2TiBr_6 exposed to ambient atmosphere (45-50% RH) are shown in Supplementary Information (Figure S8). Two additional peaks at 29.5° and 42° attributed to the CsBr phase are observed directly after removal of the protective Kapton film, suggesting a high instability of the powder in ambient atmosphere. To follow the evolution of Cs_2TiBr_6 and CsBr phases, we plot the time evolution of the maximum peak intensity for Cs_2TiBr_6 (222) at 29° and CsBr (200) at 42° along with the background intensity in Fig. 3. The maximum peak intensity of the CsBr (200) peak increases by one order of magnitude over 20 hours. Simultaneously, the maximum peak intensity of Cs_2TiBr_6 (222) remains relatively constant for 2.5 hours before decreasing toward the background signal. After 20 hours in ambient atmosphere, only CsBr peaks can be observed in the XRD spectrum (Figure S8) and a growth of the background signal is recorded, suggesting increased amorphous component in the film. Additionally, the powder exhibits hygroscopic properties (pictures given as inset in Fig. 3), consistent with the decomposition of Cs_2TiBr_6, as $TiBr_4$ and CsBr are both known to be hygroscopic.[20–22] The strong instability of the Cs_2TiBr_6 powder in ambient atmosphere for the current study is in contradiction with the results reported previously, which show similar XRD patterns of thin films before and after exposure to 80% RH for 6 hours.[8] Kong et al.[10] also observe an increase of CsBr peaks under air exposure although they do not challenge the stability of this compound.

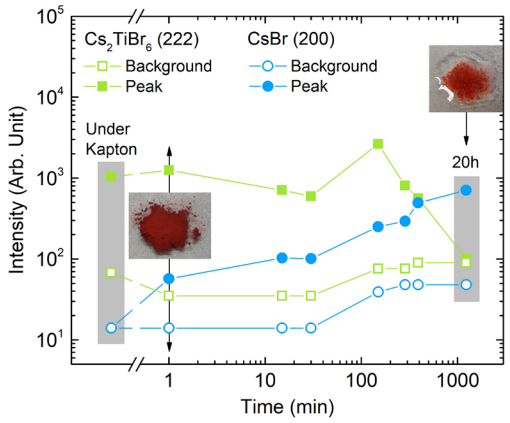

Fig. 3. Evolution of Cs_2TiBr_6 (222) and CsBr (200) peak intensities (log scale) along with the 2θ-dependent background intensity over time in ambient atmosphere after removal of the protective Kapton layer. Pictures of the Cs_2TiBr_6 powder after removal of the Kapton and after 20h of ambient atmosphere exposure are given as inset. A relative humidity RH of 45-50% was measured during the experiment.

Thermogravimetric analysis (TGA) measurement is performed on Cs_2TiBr_6 powder annealed at 100°C for two hours (Fig. 4a). The data show a very gradual 1% weight decrease as the temperature increases from 25°C to 150°C followed by a first decrease onset around 200°C and a second sharper onset at 300°C. The weight plateaus after 400°C around 64% of the initial weight. A decomposition of Cs_2TiBr_6 into CsBr and $TiBr_4$ would lead to a final weight of 54% if we consider that $TiBr_4$ evaporates. The discrepancy between the expected and observed weight losses suggests the formation of an oxide before or during the TGA measurement. XRD performed on the powder after TGA analysis (Fig. 4b) reveals a small peak at 25.5°, which may be accounted for by TiO_2 (anatase), alongside the CsBr phase. A mixture of CsBr and TiO_2 is consistent with the white color of the powder after TGA analysis. Considering that 100% of titanium in Cs_2TiBr_6 forms TiO_2 during the TGA measurement, the final weight of the TiO_2 and CsBr mixture should account for 63.7% of the initial weight, consistent with the plateau obtained after 400°C. As TGA measurement is performed under nitrogen flow and the sample is loaded within one minute of air exposure, this result suggests that Cs_2TiBr_6 is highly unstable in ambient atmosphere and reacts with oxygen to form TiO_2 at elevated temperature. To verify the role of ambient atmosphere in the decomposition of Cs_2TiBr_6 in TGA analysis, we performed XRD analysis on Cs_2TiBr_6 powder annealed at 350°C for one hour in the glovebox. The XRD pattern displayed in Fig. 4b exhibits all peaks expected for Cs_2TiBr_6, consistent with the red color of the powder after the annealing treatment. The presence of CsBr peaks and the 6% weight loss measured on the powder after thermal treatment suggest that Cs_2TiBr_6 is slowly decomposing at 350°C. Therefore, the weight loss onset around 200°C observed with TGA measurement may not be attributed to the intrinsic instability of the material but rather to the high instability of the powder in ambient atmosphere.

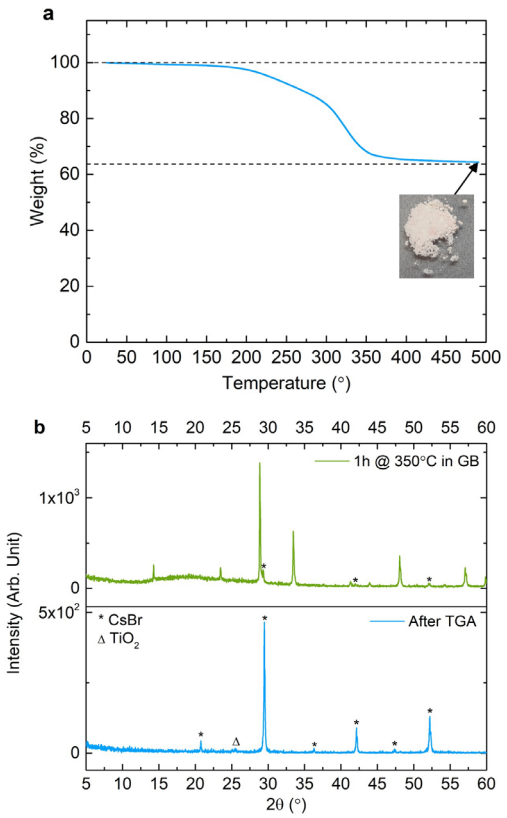

Fig. 4. (a) Thermogravimetric analysis (TGA) of Cs_2TiBr_6 powder. A picture of the powder after TGA measurement is given as inset. (b) XRD spectra of the powder after TGA analysis (bottom) and Cs_2TiBr_6 powder annealed at 350°C for 1h in the glovebox (top, XRD performed under protective Kapton film).

Conclusions

To conclude, in this work we synthesize phase pure Cs_2TiBr_6 powder using a solution synthesis approach and characterize its structure, optical properties and stability in the ambient environment. The experimental results are coupled with theoretical calculations to validate our conclusions. X-ray characterization on Cs_2TiBr_6 powder shows consistent relative peak intensities and lattice constant with predictions from the PBEsol-relaxed DFT structure. In particular, the experimental (computationally relaxed) lattice constants of 10.69 Å (10.62 Å), although different from the values previously reported[9,16], is consistent with a recent study.[10] Additionally, we show discrepancies between the previous reports[8,9] and our measured properties, as supported by DFT calculations. Solution-synthesized Cs_2TiBr_6 exhibits an experimental bandgap of between 1.9 eV (indirect) and 2.0 eV (direct) and a weak PL intensity. The absorption spectrum is consistent with DFT calculations and the PL weakness may be explained by the indirect and parity-forbidden transitions. Finally, in contradiction with the high stability reported for this compound in humid environment,[8] we show that solution-synthesized Cs_2TiBr_6 powder is highly unstable in air, as a rapid (over few hours) decomposition is observed from X-ray measurements; Strong hygroscopic properties of the powder are also observed. It is unclear at this point whether the property differences observed are due to synthetic differences among the studies (though it should be noted that, despite trying different synthetic approaches in the current study, the results for each approach were the same as those reported here) or to differences in measurement. Nevertheless, given the observations in the current study regarding band structure, measured optical properties and stability, we show that Cs_2TiBr_6 in its pristine form might not be suitable for solar energy applications.

Conflicts of interest

There are no conflicts to declare.

Acknowledgements

This work was funded in part by the Office of Energy Efficiency and Renewable Energy (EERE), U.S. Department of Energy, under Award Number DE-EE0006712 and by the National Science Foundation under Grant No. 1709294. Theoretical calculations were conducted using the resources of the National Energy Research Scientific Computing Center, which is supported by the Office of Science of the US Department of Energy under contract number DE-AC02-05CH11231.

References

1 G. Grancini, *Photoniques*, 2019, **Mars-Avril**, 24–31.
2 L. Mazzarella, Y.-H. Lin, S. Kirner, A. B. Morales-Vilches, L. Korte, S. Albrecht, E. Crossland, B. Stannowski, C. Case, H. J. Snaith and R. Schlatmann, *Adv. Energy Mater.*, 2019, **9**, 1803241.
3 H. J. Snaith, *Nat. Mater.*, 2018, **17**, 372.
4 A. K. Jena, A. Kulkarni and T. Miyasaka, *Chem. Rev.*, 2018, **119**, 3036–3103.
5 A. Jodlowski, D. Rodríguez-Padrón, R. Luque and G. de Miguel, *Adv. Energy Mater.*, 2018, **8**, 1703120.
6 T. Miyasaka, A. Kulkarni, G. M. Kim, S. Öz and A. K. Jena, *Adv. Energy Mater.*, 2019, 1902500.
7 Z. Xiao, Z. Song and Y. Yan, *Adv. Mater.*, 2019, **31**, 1803792.
8 M. Chen, M. G. Ju, A. D. Carl, Y. Zong, R. L. Grimm, J. Gu, X. C. Zeng, Y. Zhou and N. P. Padture, *Joule*, 2018, **2**, 558–570.
9 M. G. Ju, M. Chen, Y. Zhou, H. F. Garces, J. Dai, L. Ma, N. P. Padture and X. C. Zeng, *ACS Energy Lett.*, 2018, **3**, 297–304.
10 D. Kong, D. Cheng, X. Wang, K. Zhang, H. Wang, K. Liu, H. Li, X. Sheng and L. Yin, *J. Mater. Chem. C*, , DOI:10.1039/c9tc05711k.
11 G. Kresse and J. Furthmüller, *Phys. Rev. B - Condens. Matter Mater. Phys.*, 1996, **54**, 11169–11186.
12 G. Kresse and J. Furthmüller, *Comput. Mater. Sci.*, 1996, **6**.
13 P. E. Blöchl, *Phys. Rev. B*, 1994, **50**, 17953–17979.
14 P. Giannozzi, O. Andreussi, T. Brumme, O. Bunau, M. Buongiorno Nardelli, M. Calandra, R. Car, C. Cavazzoni, D. Ceresoli, M. Cococcioni, N. Colonna, I. Carnimeo, A. Dal Corso, S. de Gironcoli, P. Delugas, R. A. DiStasio Jr, A.

Ferretti, A. Floris, G. Fratesi, G. Fugallo, R. Gebauer, U. Gerstmann, F. Giustino, T. Gorni, J. Jia, M. Kawamura, H.-K. Ko, A. Kokalj, E. Kucukbenli, M. Lazzeri, M. Marsili, N. Marzari, F. Mauri, N. L. Nguyen, H.-V. Nguyen, A. Otero-de-la-Roza, L. Paulatto, S. Ponce, D. Rocca, R. Sabatini, B. Santra, M. Schlipf, A. P. Seitsonen, A. Smogunov, I. Timrov, T. Thonhauser, P. Umari, N. Vast, X. Wu and S. Baroni, *J. Phys. Condens. Matter*, 2017, **29**, 465901.

15 K. F. Garrity, J. W. Bennett, K. M. Rabe and D. Vanderbilt, *Comput. Mater. Sci.*, 2014, **81**, 446–452.

16 I. I. Kozhina and D. V. Korol'kov, *J. Struct. Chem.*, 1965, **6**, 84–89.

17 J. P. Perdew, A. Ruzsinszky, G. I. Csonka, O. A. Vydrov, G. E. Scuseria, L. A. Constantin, X. Zhou and K. Burke, *Phys. Rev. Lett.*, 2008, **100**, 136406.

18 A. E. Maughan, A. M. Ganose, M. M. Bordelon, E. M. Miller, D. O. Scanlon and J. R. Neilson, *J. Am. Chem. Soc.*, 2016, **138**, 8453–8464.

19 X. Wang, W. Meng, W. Liao, J. Wang, R. G. Xiong and Y. Yan, *J. Phys. Chem. Lett.*, 2019, **10**, 501–506.

20 R. F. Rolsten and H. H. Sisler, *J. Am. Chem. Soc.*, 1957, **79**, 5891–5893.

21 D. Punwani, C. W. Chi and D. T. Wasan, *Ind. Eng. Chem. Process Des. Dev.*, 1968, **7**, 410–415.

22 T. Boutboul, A. Breskin, R. Chechik, E. Klein, A. Braem, G. Lion and P. Miné, *Nucl. Instruments Methods Phys. Res. Sect. A Accel. Spectrometers, Detect. Assoc. Equip.*, 1999, **438**, 409–414.